Insight into strain and electronic correlation dependent magnetism in monolayer 1*T*-$CrTe_2$

Haiyan Zhu,[1] Yifan Gao,[1] Yusheng Hou,[2] Zhigang Gui,[1,3,*] and Li Huang[1,4,†]

[1]*Department of Physics, Southern University of Science and Technology, Shenzhen, Guangdong 518055, China*

[2]*Guangdong Provincial Key Laboratory of Magnetoelectric Physics and Devices, Center for Neutron Science and Technology, School of Physics, Sun Yat-Sen University, Guangzhou, 510275, China*

[3]*Academy for Advanced Interdisciplinary Studies, Southern University of Science and Technology, Shenzhen 518055, China*

[4]*Quantum Science Center of Guangdong-HongKong-Macao Greater Bay Area (Guangdong), Shenzhen 508045, China*

(Received 7 May 2023; revised 25 July 2023; accepted 20 September 2023; published 3 October 2023)

1*T*-phase $CrTe_2$ (1*T*-$CrTe_2$) has received considerable interest recently due to its high Curie temperature (T_C), which is desirable for practical spintronics applications. However, various magnetic behaviors of 1*T*-$CrTe_2$ have been reported in recent experimental and theoretical studies when its thickness reduces to ultrathin limit. In this work, the magnetic diagram of monolayer (ML) 1*T*-$CrTe_2$ with respect to in-plane biaxial strain and on-site Coulomb repulsion U is obtained based on first-principles calculations. Our results indicate that the magnetic order of ML 1*T*-$CrTe_2$ can vary among ferromagnets and antiferromagnets with strain and electronic correlation. We show that the large exchange anisotropy and higher-order biquadratic interactions are crucial to accurately describe the spin energies in ML 1*T*-$CrTe_2$. The perplexing dependencies of the magnetocrystalline anisotropy on strain and U are then well explained. Our work not only gives insight into the fundamental understanding of the unusual magnetic properties of ML 1*T*-$CrTe_2$, which is helpful to understand the diverse observations on the magnetic order in $CrTe_2$, but also sheds light on engineering their performance for spintronic devices.

DOI: 10.1103/PhysRevB.108.144404

I. INTRODUCTION

Intrinsic long-range magnetic order in recently discovered van der Waals (vdW) materials [1–4] has opened a brand-new frontier in novel spin physics. Despite a large number of two-dimensional (2D) vdW magnets reported, most of them can function only at low temperatures. For example, the Curie temperatures (T_C) of the two typical 2D magnetic materials, CrI_3 and $Cr_2Ge_2Te_6$, are 45 K [2] and 61 K [1], respectively. Tremendous efforts have been devoted to enhance the robustness of ferromagnetic (FM) order above room temperature (RT) in 2D magnets [4–8]. For example, high magnetic transition temperature can be realized in Fe_3GeTe_2 thin flakes by applying an ionic gate (∼310 K) [4] or focused ion beam (∼370 K) [8]. However, the requirements for particular device geometry and/or gating impede their practical applications. Therefore, the achievement of environmentally stable 2D magnets with their intrinsic T_Cs above RT is of great technological significance [9,10].

Cr_xTe_y is another potential family in pursuit of RT vdW magnets, particularly ferromagnetism. Among them, FM phase has been observed in layered crystal 1*T*-$CrTe_2$ with magnetic moments aligning parallel to the in-plane direction and T_C up to 310 K [11,12]. Recently, intrinsic ferromagnetism and high T_C have been experimentally demonstrated in $CrTe_2$ ultrathin films [12–15]. Most strikingly, the FM order and high critical temperature (∼200 K) are preserved in 1*T*-$CrTe_2$ with the thickness down to monolayer (ML) due to the strong perpendicular magnetic anisotropy (PMA) [13]. However, a stable zigzag antiferromagnetic (AFM) state was also observed in ML 1*T*-$CrTe_2$ grown on graphene/SiC substrate with spin-polarized scanning tunneling microscopy (SPSTM) [16]. Theoretically, varied magnetic orders including FM [17,18], zigzag AFM (AFM-Z, with $U_{\text{eff}} = 2.4$ eV) [19], striped AFM *AABB* (sAFM-*AABB*, with $U_{\text{eff}} = 3.8$ eV) [16], charge-density wave phase [20], and noncollinear magnetism [21] have been reported for ML 1*T*-$CrTe_2$, implying a strong dependence of the magnetic order on crystal structure, electronic correlation (characterized by U), as well as the cut-off distance of magnetic interactions. Controversies also exist on the magnetic easy axis of 2D 1*T*-$CrTe_2$ [13,16–18,22,23]. In contrast to its bulk counterpart, PMA has been observed in ultrathin 1*T*-$CrTe_2$ films experimentally [13,22,24]. Out-of-plane spin orientation in the yz plane with 70° off the z axis was proposed in ML 1*T*-$CrTe_2$ with SPSTM [16], while theoretical studies with $U = 2$ eV [17,18] revealed an in-plane spin orientation in ML 1*T*-$CrTe_2$. Moreover, density-functional theory (DFT) calculations [22] found that magnetic anisotropy energy changes from in plane to out of plane with increasing U. Other unusual magnetic properties like anomalous enhancement of T_C with decreasing thickness in 2D 1*T*-$CrTe_2$ are also observed [22]. In addition, the magnetic frustration driven by the competing nearest-neighbor FM direct-exchange interactions and third-nearest-neighbor AFM superexchange interactions in the triangular net of magnetic cations usually can lead to noncollinear magnetic ground

*guizg@sustech.edu.cn
†huangl@sustech.edu.cn

states, as in $NiBr_2$ and NiI_2 [25], and the biquadratic (BQ) exchange interactions have been found to play an important role to account for the novel physical phenomena in such 2D magnets [26,27]. However, for ML 1T-$CrTe_2$, which has the same triangular lattice of cations with edge-sharing octahedral coordination as $NiBr_2$ and NiI_2, only collinear magnetic states with either FM or AFM order have been proposed. To better describe the spin energies of ML 1T-$CrTe_2$, the higher-order exchange term of biquadratic interaction may be necessary when constructing the spin Hamiltonian. Therefore, it is of great importance to comprehensively investigate the strain and correlation effects for a fundamental understanding of the microscopic mechanism of the unusual magnetism exhibited in this system.

In this work, we systematically investigate the effect of strain and electronic correlations on the magnetism of ML 1T-$CrTe_2$ by using first-principles calculations. The magnetic interactions and magnetocrystalline anisotropy (MCA) are explored with different strain and on-site Coulomb repulsion U. Our results demonstrate that the magnetic order of ML 1T-$CrTe_2$ can vary among FM and AFM with strain and electronic correlations. We show that the high-order BQ exchange interactions can be crucial for the intricate magnetic orders in ML 1T-$CrTe_2$, which has been neglected in previous studies. Our work not only gives insight into understanding the unusual magnetic properties, but also reconciles some of the previous conflicting reports on the magnetic order in ML 1T-$CrTe_2$.

II. COMPUTATIONAL DETAILS

The first-principles calculations are performed within the framework of DFT using the projected augmented-wave method as implemented in the Vienna *Ab initio* Simulation Package (VASP) [28]. The exchange-correlation term is treated by the generalized-gradient approximation [29] of the Perdew-Burke-Ernzerhof functional [30]. The Kohn-Sham orbitals are expanded in a plane-wave basis set with an energy cutoff of 500 eV. The DFT+U method is employed to treat electron correlation among the localized d orbitals of Cr atoms [31,32]. Structures are fully relaxed until the forces on each atom are less than 0.01 eV/Å and the energy difference between two consecutive self-consistent steps is less than 10^{-7} eV. A k mesh of $19 \times 19 \times 1$ is used for the sampling of the Brillouin zone (BZ) of the ML primitive cell [33]. Meshes for the supercells used for magnetic properties calculations are chosen according to the mesh density for the unit cell. A vacuum space of at least 15 Å is added between the layer and its adjacent periodic images along out-of-plane axis to avoid the spurious interactions. The tight-binding (TB) analysis based on the maximally localized Wannier functions (MLWFs) are constructed from VASP *ab initio* calculations using the WANNIER90 package [34].

The MCA induced by spin-orbit coupling (SOC) is evaluated based on the total energy difference between in-plane [100] and out-of-plane [001] magnetization directions, i.e., $E_{\mathrm{MCA}} = E_{[100]} - E_{[001]}$. Here, the positive (negative) value of MCA represents out-of-pane (in-plane) magnetic easy axis. According to the second-order perturbation theory, the contribution of each orbital pair to MCA can be written as

$$\Delta E_{\mathrm{MCA}} = E^{\sigma\sigma'}(x) - E^{\sigma\sigma'}(z) = (2\delta_{\sigma\sigma'} - 1)\xi^2 \sum_{o^\sigma, u^{\sigma'}} \frac{|\langle o^\sigma | L_z | u^{\sigma'} \rangle|^2 - |\langle o^\sigma | L_x | u^{\sigma'} \rangle|^2}{E_u^{\sigma'} - E_o^{\sigma}}, \quad (1)$$

where ξ is the SOC constant; o and u represent the occupied and unoccupied state, respectively; and σ and σ' are the different spin states.

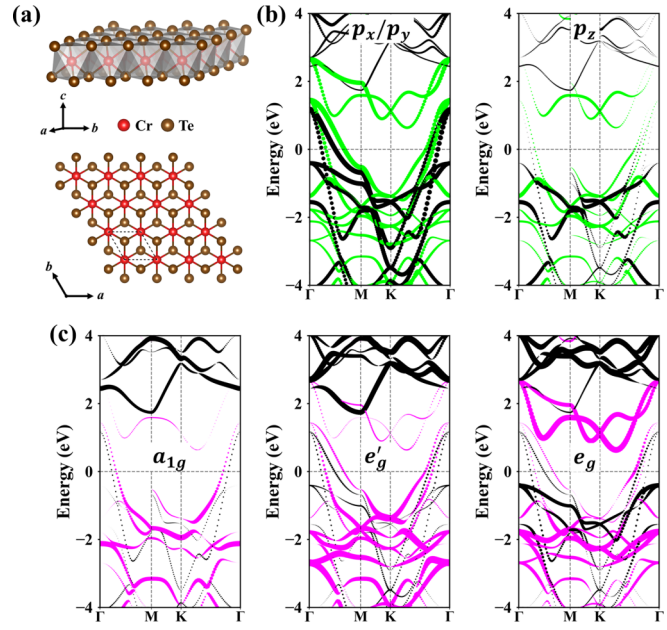

FIG. 1. (a) Top and side view of ML 1T-$CrTe_2$. (b) Spin-polarized projected band structures of Te p orbitals with $U = 3$ eV. Green (black) dots represent the spin-up (down) channel. (c) Spin-polarized projected band structures of Cr d orbitals with $U = 3$ eV. Magenta (black) dots represent spin-up (down) channel.

III. RESULTS AND DISCUSSION

A. Geometrics and electronic structure of ML 1T-$CrTe_2$

The bulk 1T-$CrTe_2$ compound crystallizes in layered CdI_2-type structure with space group $P\bar{3}m1$ (No. 164) [11]. The crystal structure of ML 1T-$CrTe_2$ shares the same symmetry as the bulk, in which one Cr atomic layer is sandwiched by two Te atomic layers, as shown in Fig. 1(a). The calculated lattice constant (a_{DFT}) with $U = 3$ eV is 3.71 Å, which is 2.3% smaller than the experimental value (a_{exp})$\sim$ 3.80 Å of 2D 1T-$CrTe_2$ [15,22], but is quite consistent with other theoretical results [17,18]. Since each Cr atom is surrounded by six Te atoms forming a local octahedral coordination but trigonal crystal field in the global coordinate system, the triplet t_{2g} states of Cr split into one singlet a_{1g} and one doublet e'_g orbital with the local-symmetry point group of the Cr atoms lowered from O_h to D_{3d} (see Fig. S1 of the Supplemental Material (SM) [35]). The a_{1g}, e'_g, and e_g states can be expressed by the linear combination of the five d orbitals for perfect octahedral

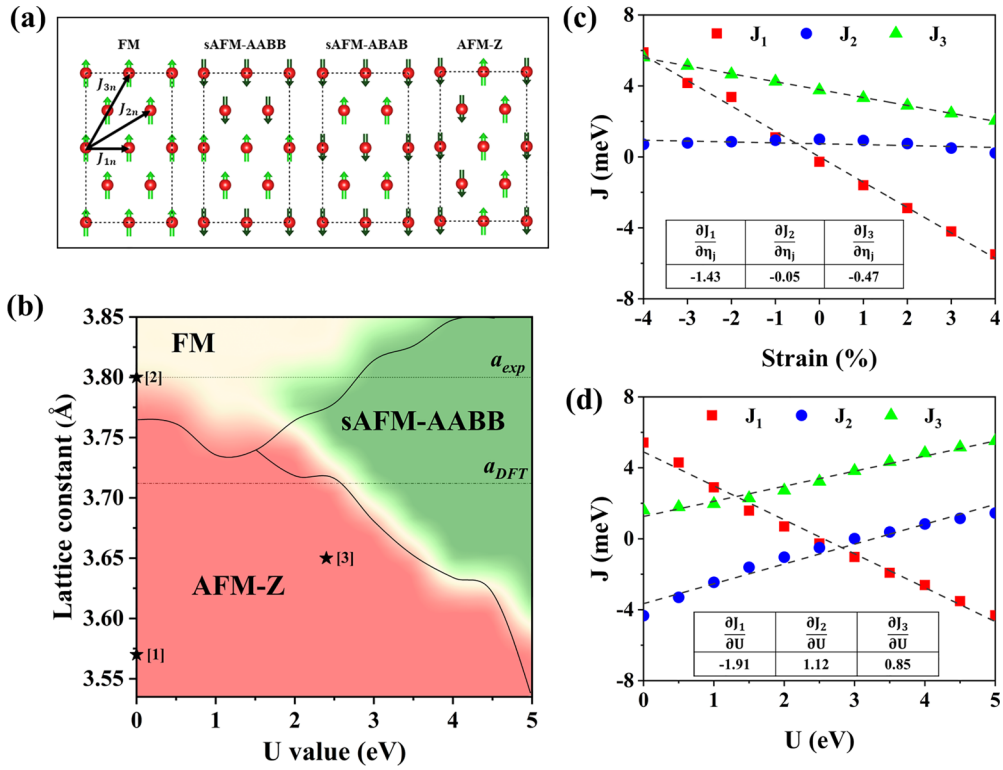

FIG. 2. Strain and electronic correlation effect on magnetism of ML 1T-$CrTe_2$. (a) Top view of four magnetic configurations. Black arrows denote first-, second-, and third-nearest-neighbor exchange interactions J_1, J_2, and J_3. Positive (negative) values represent AFM (FM) interaction. Only Cr atoms are visible here for simplicity. (b) Diagram of DFT-calculated magnetic ground state with varied lattice constant and U. Red, green, and yellow represent AFM-Z, sAFM-$AABB$, and FM magnetic ground state, respectively. Phase boundaries indicated by black solid lines are just for eye guidance. Gray dot lines label lattice constant of a_{DFT} and a_{exp}. Black stars [1]∼ [3] mark lattice constant and U adopted in Ref. [37], Ref. [13], and Ref. [19], respectively. (c) Exchange parameters as function of biaxial strain with $U = 3$ eV, and (d) exchange parameters as function of U with lattice constant of a_{DFT}. Dashed black lines are fitted lines. Inset tables list first-order derivatives of exchange parameters with respect to strain or U.

field [36]:

$$e_g \begin{cases} e_{g1} = \frac{1}{\sqrt{3}} d_{xy} - \frac{\sqrt{2}}{\sqrt{3}} d_{xz} \\ e_{g2} = \frac{1}{\sqrt{3}} d_{x^2-y^2} - \frac{\sqrt{2}}{\sqrt{3}} d_{yz} \end{cases} \qquad e'_g \begin{cases} e'_{1g} = \frac{\sqrt{2}}{\sqrt{3}} d_{xy} + \frac{1}{\sqrt{3}} d_{xz} \\ e'_{2g} = \frac{\sqrt{2}}{\sqrt{3}} d_{x^2-y^2} + \frac{1}{\sqrt{3}} d_{yz} \end{cases} \qquad a_{1g} = d_{z^2} \,, \tag{2}$$

where the xyz coordinate is the global axis with x (z) directed along the a (c) crystallographic axis; then, the y axis is uniquely defined. Our calculated magnetic moment per Cr atom is $\sim 3.3\mu_B$ parallelly occupying the low-energy states a_{1g} and e'_g as well as slightly partial e_g when $U = 3$ eV [see Fig. 1(c)], which is in good agreement with both experimental results [13] and theoretical calculations [18,20]. This suggests that the Cr atoms in ML 1T-$CrTe_2$ is in the d^3 configuration with $\sim 3\mu_B$ magnetic moments. The Fermi level (E_F) crosses the heavily hybridized bands between Cr d orbitals and Te p orbitals, resulting in the metallic character of ML 1T-$CrTe_2$ [see Figs. 1(b) and 1(c)].

B. Strain and U-dependent magnetic interactions of ML 1T-$CrTe_2$

To determine the magnetic ground state of the ML 1T-$CrTe_2$, we calculate the relative total energies of four different magnetic configurations [i.e., FM, sAFM-$AABB$, sAFM-$ABAB$, and AFM-Z] [see Fig. 2(a)] under different biaxial strain with U changing from 0 to 5 eV. To accommodate the four magnetic configurations, a $2 \times 2\sqrt{3} \times 1$ rectangular supercell [Fig. 2(a)] is used. The strain dependence of the relative total energies of the four magnetic configurations for $U = 0 \sim 5$ eV are shown in Fig. S2 of the SM [35]. It can be seen that the strain and electronic correlations can strongly influence the magnetic ground states of ML 1T-$CrTe_2$, giving rise to a complex magnetic diagram with respect to the strain and electronic correlations [Fig. 2(b)]. We note that our results give the same magnetic orders with the particular lattice constants and U adopted in previous studies [13,19,37], which are marked as asterisks in Fig. 2(b). It can be seen that the ML 1T-$CrTe_2$ prefers a FM order in the region with enlarged lattice constant (>3.8 Å) and U is smaller than 4 eV. For the structure optimized at a_{exp}, when U is smaller than 2.5 eV, the magnetic ground is FM; otherwise, the sAFM-AABB

is the most stable state. While for the structure with a_{DFT}, the magnetic ground state is in the AFM-Z configuration, which changes to sAFM-*AABB* order when U is larger than 3.0 eV. The enlarged sAFM-*AABB* region under an increased U value is qualitatively consistent with the results reported in Ref. [19].

We now investigate the role of strain in tunning the magnetic properties of ML 1T-$CrTe_2$. The phonon dispersions of ML 1T-$CrTe_2$ with both a_{DFT} and a_{exp} are checked within $0 \sim 5$ eV for U (see Fig. S3 of SM [35]). The ML 1T-$CrTe_2$ demonstrates dynamic stability for U values ranging from 2 to 4 eV, which is consistent with previous theoretical studies [16–19]. The magnetic interactions under different in-plane biaxial strains are analyzed in detail using the value of $U = 3$ eV. We start our analysis from fitting the first-order derivatives of exchange parameters with respect to strain. Magnetic exchange parameters are obtained using both the energy-mapping method and four-state method (see Supplemental Note 1 and Table SI of SM [35] for more details). Both approaches show that the third-nearest-neighbor exchange parameter (J_3) in ML 1T-$CrTe_2$ is significant, which is common in magnetic materials with similar triangle magnetic structure [27,38]. Interestingly, the first-nearest-neighbor exchange parameter (J_1) is found to be smaller compared to J_3, which may be ascribed to multiple factors, such as itinerant electrons and the competitions between superexchange and direct exchange. See Supplemental Note 2 in SM [35] for more detailed explanations. The strain dependence of J_i ($i = 1, 2, 3$) is shown in Fig. 2(c). It can be seen that the first-order derivatives of J_1 (i.e., $\frac{\partial J_1}{\partial \eta_j}$) and J_3 (i.e., $\frac{\partial J_3}{\partial \eta_j}$) are negative, indicating that ferromagnetism in ML 1T-$CrTe_2$ is enhanced under tensile strain, and the very small value of $\frac{\partial J_2}{\partial \eta_j}$ suggests that the J_2 is insensitive to in-plane strain. It is also interesting to note that the magnitude of $\frac{\partial J_1}{\partial \eta_j}$ is approximately 3 times larger than that of $\frac{\partial J_3}{\partial \eta_j}$.

To get further insight into this behavior, we decompose the total first-order spin-lattice (SL) coupling strength $\frac{\partial J_{\mu\mu'}}{\partial \eta_j}$ into contributions from each atom using the method proposed in Ref. [39]. We classify all the atoms into three types: the magnetic Cr-Cr pair, the bridging Te (Te^B) of the selected Cr-Cr pair, and the environmental Te (Te^E). As shown in Table I, for the nearest Cr pair, the contributions to $\frac{\partial J_1}{\partial \eta}$ from Cr and Te^E are negative, which implies the strain-enhanced ferromagnetism in ML 1T-$CrTe_2$. Strikingly, the overall positive contribution to the ferromagnetism from $\frac{\partial J_3}{\partial \eta}$ is considerable but much smaller than that from $\frac{\partial J_1}{\partial \eta}$, which explains why J_3 is less sensitive to strain than J_1. More details about this method and analyses are given in the Supplemental Note 3 of SM [35].

To get a better understanding of the strain sensitivity of the magnetic exchange parameters, we further perform a tight-binding analysis. The magnetism of ML 1T-$CrTe_2$ is a result of competition between the direct Cr d–d hopping and the superexchange interactions mediated through the bridging ligands Te. The direct-exchange interaction favors AFM order, while the superexchange coupling near the 90° bond angles favors FM order according to the Goodenough-Karamori-Anderson (GKA) rules [40,41]. The variation of Js with strain can be characterized by the ratio between the gradients of hopping terms (Δt) and the corresponding hopping parameters in the absence of strain (t_0), i.e., $\frac{\Delta t}{t_0}$. Here, we mainly focus on the main hopping channel $d_{x^2-y^2} - d_{x^2-y^2}$ and $p_x - d_{xz}$, which is found to be responsible for the AFM and FM coupling, respectively (see Table SII). These hopping parameters as a function of strain are calculated by constructing the MLWFs, which are shown in Fig. S6(a) in SM [35], and their derivatives relative to t_0 are shown in Fig. 3(a). It can be found that $\frac{\Delta t_{dd}}{t_{dd}}$ (-5.57) is much larger than $\frac{\Delta t_{pd}}{t_{pd}}$ (-1.89), which means the AFM direct-exchange interactions decrease considerably faster than the FM superexchange interactions. The possible reason for the smaller $|\frac{\Delta t_{pd}}{t_{pd}}|$ could be that the Cr-Te-Cr angle ($\theta_{\text{Cr-Te-Cr}}$) gets closer to 90°, thus enhancing the FM coupling to some degree, while the obviously enlarged Cr-Cr distance ($d_{\text{Cr-Cr}}$) with strain largely suppresses the AFM direct interaction [see Fig. 3(c)].

TABLE I. First-order exchange derivatives $\frac{\partial J}{\partial u}$ (meV/Å) and their contributions to first-order SL coupling strength $\frac{\partial J}{\partial \eta}$ (meV/%).

Ion	$\frac{\partial J_1}{\partial u_x}$	$\frac{\partial J_1}{\partial u_y}$	$\frac{\partial J_1}{\partial u_z}$	$\frac{\partial J_1}{\partial \eta}$
Cr	−3.58	6.21	0.00	−9.98
Te^B	−7.45	−4.30	−14.50	8.85
Te^{E1}	−1.77	5.33	1.47	−14.50
Te^{E2}	−3.71	4.19	−1.47	−18.44
Ion	$\frac{\partial J_2}{\partial u_x}$	$\frac{\partial J_2}{\partial u_y}$	$\frac{\partial J_2}{\partial u_z}$	$\frac{\partial J_2}{\partial \eta}$
Cr	0.00	−2.75	−0.74	6.30
Cr^E	−1.52	0.00	0.00	2.82
Te^B	0.00	−1.87	0.31	−1.43
Ion	$\frac{\partial J_3}{\partial u_x}$	$\frac{\partial J_3}{\partial u_y}$	$\frac{\partial J_3}{\partial u_z}$	$\frac{\partial J_3}{\partial \eta}$
Cr	−2.24	3.88	0.00	12.47
Te^{B1}	−3.89	5.50	1.27	−14.10
Te^{B2}	−2.82	6.11	−1.27	−5.84

To get further insight into this behavior, we decompose the total first-order spin-lattice (SL) coupling strength $\frac{\partial J_{\mu\mu'}}{\partial \eta_j}$ into contributions from each atom using the method proposed in Ref. [39]. We classify all the atoms into three types: the magnetic Cr-Cr pair, the bridging Te (Te^B) of the selected Cr-Cr pair, and the environmental Te (Te^E). As shown in Table I, for the nearest Cr pair, the contributions to $\frac{\partial J_1}{\partial \eta}$ from Cr and Te^E are negative, which implies the strain-enhanced ferromagnetism in ML 1T-$CrTe_2$. Strikingly, the overall positive contribution to the ferromagnetism from $\frac{\partial J_3}{\partial \eta}$ is considerable but much smaller than that from $\frac{\partial J_1}{\partial \eta}$, which explains why J_3 is less sensitive to strain than J_1. More details about this method and analyses are given in the Supplemental Note 3 of SM [35].

To get a better understanding of the strain sensitivity of the magnetic exchange parameters, we further perform a tight-binding analysis. The magnetism of ML 1T-$CrTe_2$ is a result of competition between the direct Cr d–d hopping and the superexchange interactions mediated through the bridging ligands Te. The direct-exchange interaction favors AFM order, while the superexchange coupling near the 90° bond angles favors FM order according to the Goodenough-Karamori-Anderson (GKA) rules [40,41]. The variation of Js with strain can be characterized by the ratio between the gradients of hopping terms (Δt) and the corresponding hopping parameters in the absence of strain (t_0), i.e., $\frac{\Delta t}{t_0}$. Here, we mainly focus on the main hopping channel $d_{x^2-y^2} - d_{x^2-y^2}$ and $p_x - d_{xz}$, which is found to be responsible for the AFM and FM coupling, respectively (see Table SII). These hopping parameters as a function of strain are calculated by constructing the MLWFs, which are shown in Fig. S6(a) in SM [35], and their derivatives relative to t_0 are shown in Fig. 3(a). It can be found that $\frac{\Delta t_{dd}}{t_{dd}}$ (-5.57) is much larger than $\frac{\Delta t_{pd}}{t_{pd}}$ (-1.89), which means the AFM direct-exchange interactions decrease considerably faster than the FM superexchange interactions. The possible reason for the smaller $|\frac{\Delta t_{pd}}{t_{pd}}|$ could be that the Cr-Te-Cr angle ($\theta_{\text{Cr-Te-Cr}}$) gets closer to 90°, thus enhancing the FM coupling to some degree, while the obviously enlarged Cr-Cr distance ($d_{\text{Cr-Cr}}$) with strain largely suppresses the AFM direct interaction [see Fig. 3(c)].

The origin of the enhanced FM behavior can be further understood based on the evolution of electronic properties with strain near the E_F. A schematic representation of the (near-)90° superexchange interactions is shown in Fig. 3(e). Assuming that the spin of Cr1 d is up aligned, then charge transfer occurs from Te $p\uparrow$ state to Cr1 $e_g\uparrow$ state. The remaining $p\downarrow$ state will interact with Cr2 $a_{1g}\downarrow$ state, leading to FM coupling between Cr1 and Cr2 to ensure the lowest energy cost. When the in-plane biaxial strain is applied, the p orbitals of Te atom are elevated and obviously reduce the energy difference between the p state and the $e_g\uparrow$ ($a_{1g}\downarrow$) state of the Cr1 (Cr2) and a subsequence enhancement in FM interactions.

More comprehensive details regarding geometric changes, such as alterations in bond lengths and angles, as well as the modifications of electronic structures impacting the magnetic exchange interactions, can be found in Supplemental Note 4 in SM [35].

Given the controversial experimental observations [13,16], it becomes challenging to ascertain a specific U value for ML 1T-$CrTe_2$. On the other hand, the electron correlation effects are generally more pronounced in 2D limit as the electronic

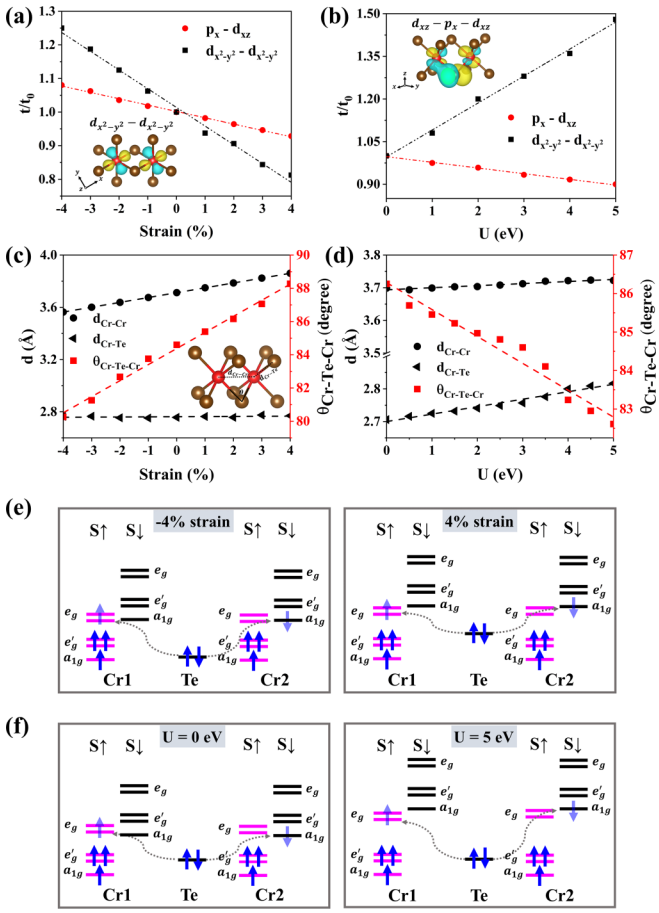

FIG. 3. Relative change of hopping term t/t_0 with (a) strain and (b) U. Only main dd and pd hopping channels are shown for simplicity. Wannier orbitals of corresponding hopping channels are shown as insets. Cr-Cr distance ($d_{\text{Cr-Cr}}$), Cr-Te distance ($d_{\text{Cr-Te}}$), and Cr-Te-Cr angle ($\theta_{\text{Cr-Te-Cr}}$) with respect to (c) strain and (d) U. (e) Schematic representation of (near-) 90° Cr1 d - Te p - Cr2 d superexchange interaction under 4% compressive strain (left) and 4% tensile strain (right). Panel (f) is similar to panel (e) but for $U = 0$ eV (left) and $U = 5$ eV (right).

screening substantially weakens in 2D systems. For some 2D magnets, the magnetic properties are found to be robust with electronic correlation [42,43], while for some magnetic metals (such as in $CrTe_2$), the correlation effect could be tricky. It is thus necessary and intriguing to perform a systematical study on the role of electronic correlations in the magnetism of monolayer 1T-$CrTe_2$ by varying the on-site Coulomb repulsion U parameter. Although $\frac{\partial J_1}{\partial U}$ is negative, both $\frac{\partial J_2}{\partial U}$ and $\frac{\partial J_3}{\partial U}$ are positive, suggesting the possibility of enhanced AFM interactions with increasing U. Similarly, the variation of Js with U can be characterized by the ratio between the gradients of hopping terms (Δt) and the corresponding hopping parameters. It is confirmed by the remarkable positive $\frac{\Delta t_{dd}}{t_{dd}}$ compared with negative $\frac{\Delta t_{pd}}{t_{pd}}$, as can be seen in Fig. 3(b). The $\theta_{\text{Cr-Te-Cr}}$ deviates from 90° with U [see Fig. 3(d)], which is a sign for weakened FM superexchange interactions. The electronic correlations can also strongly influence the electronic structures of materials with d orbitals. In Fig. 3(f), we schematically display the exchange mechanism with increasing U. The energy difference between Te p state and Cr1 $e_g \uparrow$ (Cr2 $a_{1g} \downarrow$) state increases with increasing U from 0 to 5 eV. The FM superexchange interactions are then suppressed, and the AFM direct-exchange interactions become dominate with a large U value.

C. The role of biquadratic exchange interactions in ML 1T-$CrTe_2$

Based on the exchange parameters discussed above, magnetic frustration may exist due to the competition between the FM (negative J_1) and AFM (positive J_3) coupling in the ML 1T-$CrTe_2$. Therefore, we perform the spin dynamics Monte Carlo simulations to check the ground state of ML 1T-$CrTe_2$ based on only bilinear exchange interactions. A noncollinear state is obtained as expected, which is also consistent with the previous report [21]. To understand the experimentally observed collinear FM or AFM magnetic ground state in ML 1T-$CrTe_2$, rather than any noncollinear phase, we carry out DFT spin spirals calculations using a generalization of Bloch condition [44] as implemented in VASP and study the excitations of the given spin Hamiltonian based on the linear spin-wave theory (LSWT) with different exchange combinations using SPINW package [45]. To better describe the four magnetic configurations, an orthogonal magnetic cell with two Cr atoms is used. The diagram of the four magnetic configurations in the orthogonal cell is shown in Fig. S7 of SM [35]. Two cases are considered here: (i) the two Cr atoms are parallel aligned, and the FM, sAFM-*AABB*, and AFM-*Z* order are then labeled as @orth- ↑↑ -Γ, @orth- ↑↑ -Y, and @orth- ↑↑ -X, respectively; (ii) the two Cr atoms are antiparallel aligned, and the sAFM-*AABB* and sAFM-*ABAB* order are then labeled as @orth- ↑↓ −Y and @orth- ↑↓ -Γ, respectively. The DFT calculated total energies of the case (i) with lattice constant a_{DFT} and $U = 3$ eV as a function of magnetic propagation vector q are presented in Fig. 4(a). It can be seen that the energy minimum located at the Y point in the first BZ, which indicates that sAFM-*AABB* is the ground state.

For comparison, we first employ the LSWT analysis using a standard bilinear Heisenberg spin Hamiltonian:

$$H = \mathcal{J}_1 \sum_{ij} \vec{S}_i \cdot \vec{S}_j + \mathcal{J}_2 \sum_{ik} \vec{S}_i \cdot \vec{S}_k + \mathcal{J}_3 \sum_{il} \vec{S}_i \cdot \vec{S}_l + A_i \sum_i \left(\vec{S}_i^z\right)^2, \quad (3)$$

where $\mathcal{J}_1$, $\mathcal{J}_2$, and $\mathcal{J}_3$ represent the first-, second-, and third-nearest-neighbor exchange interactions, respectively. A_i is the single-ion anisotropy, and $\vec{S}_i^z$ is the z component of the spin vector. Here, we consider two situations: one is the isotropy case without inclusion of the SOC (J_{123}) and the other one is the 3 × 3 magnetic exchange tensor with exchange anisotropy involved ($\mathbb{J}_{123}$). The magnitude of $\mathbb{J}_{123}$ and A of ML 1T-$CrTe_2$ are collected in Table II. The positive A favors an in-plane orientation of the spin, in good agreement with existing theoretical results [17,18]. The q-dependent spin energies based on Eq. (3) are shown in Fig. 4(b). A comparison of Figs. 4(a) and 4(b) suggests that the exchange anisotropy in ML 1T-$CrTe_2$ is salient since the energy curves from $\mathbb{J}_{123} + A$ fit better

TABLE II. Exchange-coupling parameters for ML 1T-$CrTe_2$. Tensor elements, in global $\{x, y, z\}$ basis, of first- ($\mathbb{J}_1$), second- ($\mathbb{J}_2$), and third-nearest-neighbor ($\mathbb{J}_3$) spins. Spin pairs used for calculation of $\mathbb{J}_1$, $\mathbb{J}_2$, and $\mathbb{J}_3$ are presented in Fig. S4. Single-ion anisotropy (A), and first-nearest BQ interaction (K_{B1}) are also listed.

Tensile strain	$\mathbb{J}_1$ (meV)	$\mathbb{J}_2$ (meV)	$\mathbb{J}_3$ (meV)	A (meV)	K_{B1} (meV)
0%	$\begin{pmatrix} -1.79 & 0.19 & -0.39 \\ 0.19 & -1.99 & -0.23 \\ -0.39 & -0.23 & -1.56 \end{pmatrix}$	$\begin{pmatrix} 0.62 & 0.00 & 0.00 \\ 0.00 & 0.48 & -0.02 \\ 0.00 & -0.02 & -0.10 \end{pmatrix}$	$\begin{pmatrix} 3.03 & 0.02 & 0.01 \\ 0.02 & 3.00 & 0.01 \\ 0.02 & 0.01 & 3.10 \end{pmatrix}$	1.95	−0.64
5%	$\begin{pmatrix} -9.21 & 0.13 & -0.38 \\ 0.13 & -9.36 & -0.22 \\ -0.38 & -0.22 & -9.15 \end{pmatrix}$	$\begin{pmatrix} 0.00 & 0.09 & 0.04 \\ 0.00 & -0.37 & 0.03 \\ -0.37 & 0.03 & -0.49 \end{pmatrix}$	$\begin{pmatrix} 2.03 & 0.09 & 0.04 \\ 0.09 & 1.93 & 0.03 \\ 0.04 & 0.03 & 1.81 \end{pmatrix}$	−0.03	−0.45

with the DFT results than that from $J_{123} + A$. However, such a $\mathcal{J}_{123} + A$ model is still inadequate to describe the spin energies of strain-free ML 1T-$CrTe_2$ correctly. The minimum of $E(q)$ curve occurs at $q = (0.17, 0.5, 0)$, and the energy difference between $E(0.17, 0.5, 0)$ and $E(0, 0.5, 0)$ is as large as 3.83 (1.90) meV/Cr for $J_{123} + A$ ($\mathbb{J}_{123} + A$) case, suggesting that other additional exchange interactions may play a part in the magnetism of ML 1T-$CrTe_2$. We thus further consider the BQ exchange interactions in this system, which have been proposed to be non-negligible when exploring the magnetic properties in 2D magnets [26], especially when magnetic frustration is present [27], but has not been discussed so far for ML 1T-$CrTe_2$, to the best of our knowledge. As shown in Figs. 4(a), 4(b), and Table II, there is considerable magnetic exchange anisotropy/frustration. Additionally, the energy difference between the collinear and noncollinear states around the Y point [in Fig. 4(b)] is small, which is comparable to the biquadratic exchange energy. To demonstrate it, the spin Hamiltonian with the nearest BQ exchange interactions (K_{B1}) included is now described as follows:

$$H = \sum_{ij}[\mathcal{J}_1 \vec{S}_i \cdot \vec{S}_j + K_{B1}(\vec{S}_i \cdot \vec{S}_j)^2] + \mathcal{J}_2 \sum_{ik} \vec{S}_i \cdot \vec{S}_k + \mathcal{J}_3 \sum_{il} \vec{S}_i \cdot \vec{S}_l + A_i \sum_i \left(\vec{S}_i^z\right)^2. \quad (4)$$

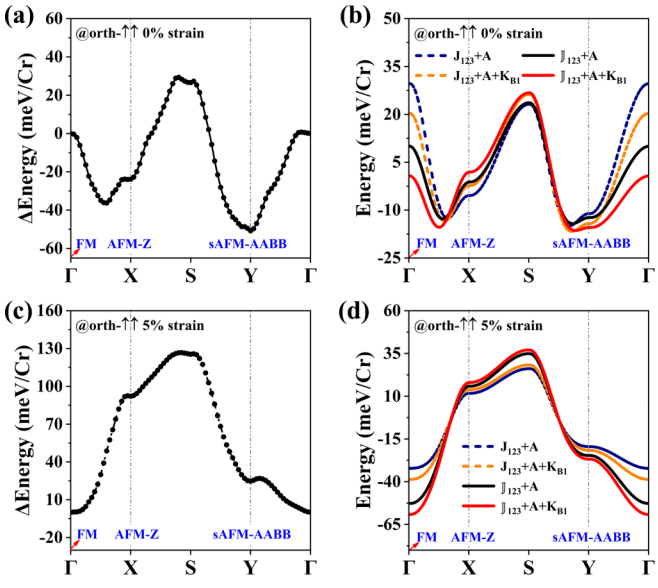

FIG. 4. Energetics of magnetic states for orthogonal cell of ML 1T-$CrTe_2$ with two Cr atoms parallel aligned. Relative total energy dependence on magnetic propagation vector q at (a) 0% and (c) 5% tensile strain with $U = 3$ eV, respectively. Energy of FM state is chosen as reference. Dependence of spin energies on q based on LSWT at (b) 0% and (d) 5% tensile strain with $U = 3$ eV, respectively.

As shown in Table II, the magnitude of the calculated K_{B1} is larger than that reported for most 2D magnets [26,27]. The inclusion of BQ exchange interactions (K_{B1} term) adds a renormalized part to the bilinear exchange interactions by adding $2S(S-1)K_{B1}$ to $\mathcal{J}_1$ according to LSWT [45]. Strikingly, the negative K_{B1} is found to contribute to the stabilization of the FM and sAFM-*AABB* states, and their energies are largely decreased by 9.32 and 3.11 meV/Cr, respectively, with the K_{B1} included, while the AFM-Z and sAFM-*ABAB* become energetically unfavorable (see Fig. 4(b) and Fig. S8(b) of SM [35]). To clearly see how the energy difference between sAFM-*AABB* and the spin configuration with lowest energy in the q range of S–Y ($\Delta E = E_{\text{sAFM-AABB}} - E_{\min}$) changes with K_{B1}, we artificially change the magnitude of K_{B1} by multiplying a factor α. As shown in Fig. S9 of SM [35], the sAFM-*AABB* state gets more stable with enhancing K_{B1}, and finally becomes the magnetic ground state when K_{B1} is 6 times the original DFT result.

Considering the large SL coupling in ML 1T-$CrTe_2$, the above analyses are also performed for ML 1T-$CrTe_2$ with 5% tensile strain (see Figs. 4(c) and 4(d) and Figs. S8(c) and S8(d) of SM [35]). It can be seen that FM is the magnetic ground state whether K_{B1} is included or not, which is consistent with the strain effect on the magnetic exchanges in Sec. III B. Moreover, it is worth noting that the energy difference between FM and AFM-Z (as well as sAFM-*AABB*) from the $\mathbb{J}_{123} + A + K_{B1}$ model fits better with the DFT results, indicating that the exchange anisotropy and BQ interactions are important in ML 1T-$CrTe_2$. However, we also note that in contrast to the DFT spiral calculation results, inclusion of K_{B1} alone still fails to give the lowest-energy phase sAFM-*AABB* in the strain-free situation, which implies other higher-order exchange interactions or noncollinear phenomena may play roles in ML 1T-$CrTe_2$ and is beyond the scope of this work.

D. Strain and U-dependent MCA of ML 1T-$CrTe_2$

The sign of magnetic anisotropy of ML 1T-$CrTe_2$ is also a controversial issue in both experimental data [16,22] and theoretical predictions [17,19,20,46], which also

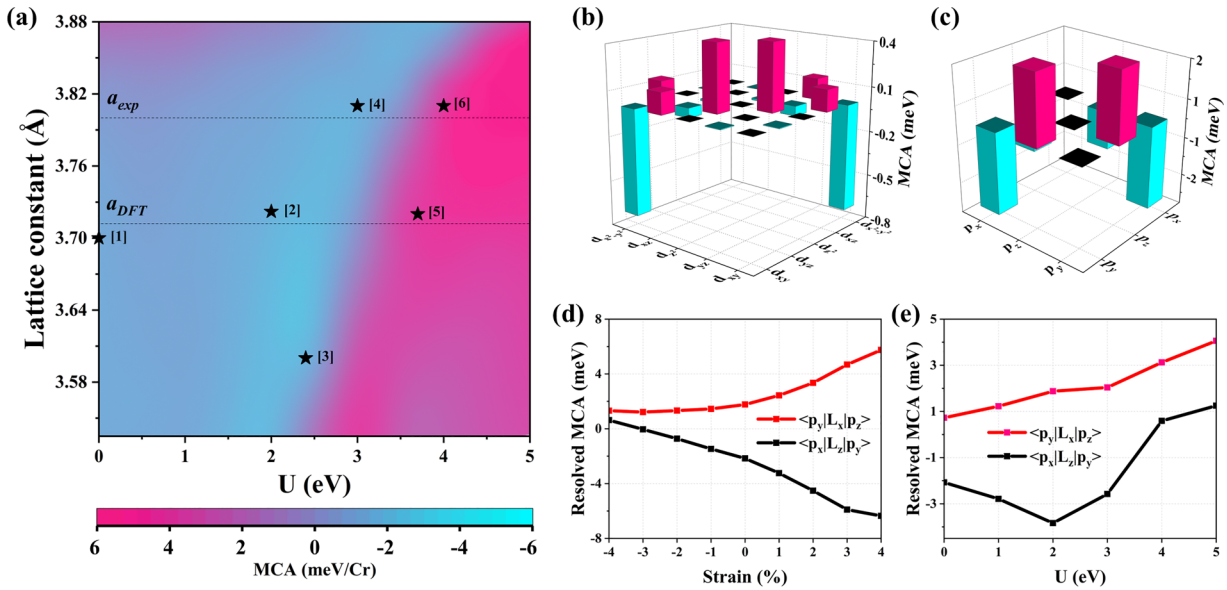

FIG. 5. (a) MCA diagram of ML 1T-$CrTe_2$ with respect to lattice constant and U. Black stars [1]∼ [6] mark lattice constant and U used in Ref. [20], Ref. [17], Ref. [19], Ref. [22], Ref. [46], and Ref. [22], respectively. Orbital-resolved MCA of (b) Cr d and (c) Te p orbitals of ML 1T-$CrTe_2$ with lattice constant of a_{DFT} and $U = 3$ eV. Orbital-resolved MCA of Te p orbitals as function of (d) strain with $U = 3$ eV and (e) U at lattice constant of a_{DFT}, for which only orbital pairs mostly affected by strain and U are presented.

suggests a sensitivity of the MCA to strain and screening in ML 1T-$CrTe_2$. To address this question, we now explore the effect of strain and electronic correlations on the MCA of this system. Figure 5(a) shows the calculated MCA diagram with respect to lattice constant and U. For comparison, previous reported data [17,19,20,22,46] are also marked as stars in Fig. 5(a). It can be clearly seen that the MCA of ML 1T-$CrTe_2$ is indeed very sensitive to U value. When U is smaller (larger) than 3.0 (3.5) eV, the ML 1T-$CrTe_2$ prefers in-plane (out-of-plane) magnetic easy axis in a sizable strain range. Most notably, the FM order region in the magnetic diagram of Fig. 2(b) mainly lies in the positive MCA region of $0.0 \sim 2.0$ meV/Cr in Fig. 5(a), which agrees with the experimental observations of intrinsic ferromagnetism and PMA for ML 1T-$CrTe_2$ [13,22].

To reveal the electronic origin of the calculated MCA, we resolve the MCA into the SOC energies between each orbital pair for Cr d and Te p, which are shown in Fig. 5(b). It is found that the contribution from Cr atoms is much smaller than that from Te atoms, as expected due to the stronger SOC strength in Te. The orbital angular momenta L of Cr and Te atoms are also calculated, which shows that the main unquenched L around E_F are from Cr L_z and Te L_x, L_z (see Fig. S10 of SM [35]). The projected band structures shown in Figs. 1(b) and 1(c) indicate that the occupied states and unoccupied states of Cr d orbitals near the E_F are both from the spin-up channel ($\delta_{\sigma\sigma'} = 1$, spin-conserving case), while they are mainly from the opposite spin channel ($\delta_{\sigma\sigma'} = 0$, spin-flipping case) for Te p orbitals. Thus, the magnitudes of the second-order contribution to MCA are given by

$$\Delta E(e_g'^{+} e_g^{+}) = \sum_{o^+,u^+} \frac{|\langle e_g'^{+}|L_z|e_g^{+}\rangle|^2 - |\langle e_g'^{+}|L_x|e_g^{+}\rangle|^2}{\epsilon_{u^+} - \epsilon_{o^+}}, \quad (5)$$

$$\Delta E(p_y^-,\ p_x^+) = (-1) \sum_{o^-,u^+} \frac{|\langle p_y^-|L_z|p_x^+\rangle|^2 - |\langle p_y^-|L_x|p_x^+\rangle|^2}{\epsilon_{u^+} - \epsilon_{o^-}}, \quad (6)$$

where the superscript + (−) denotes spin-up (down) state. Therefore, for spin-flipping transition in Te p orbitals, SOC elements between occupied and unoccupied states through the L_z (L_x) operator contribute to negative (positive) MCA. For spin-conserving case in Cr d orbitals, the contribution to MCA is reversed. Since the magnitude of Te L_z is obviously larger than Te L_x (see Figs. S10(d) and S10(f) of SM [35]), which thus results in the negative MCA and in-plane magnetic anisotropy with lattice constant of a_{DFT} and $U = 3$ eV, as mentioned above.

We further investigate the strain dependence of MCA with a fixed value of $U = 3$ eV. As shown in Figs. 5(a) and S11(a) of SM [35], the MCA becomes positive under compressive strain and increases monotonically, while in-plane magnetic easy axis is stabilized under tensile strain. In order to obtain insight into the role of strain on MCA in this system, we plot the projected band structure of Cr d states and density of states of Te p states under −4 and 4% strain, respectively (see Fig. S12 of SM [35]). Based on Eq. (5), one can see that both the positive contribution from spin-conserving transition $|\langle e_g'^{+}|L_z|e_g^{+}\rangle|^2$ (red arrow in Fig. S12(a) of SM [35]) and the negative contribution from spin-flipping transition $|\langle e_g'^{+}|L_z|e_g'^{-}\rangle|^2$ (blue arrow in Fig. S12(a) of SM [35]) from Cr d states are almost unchanged with strain, which is less likely the origin of the change in MCA. For Te p states, the negative (positive) contributions from spin-flipping transition $|\langle p_y^-|L_z|p_x^+\rangle|^2$ ($|\langle p_y^-|L_x|p_z^+\rangle|^2$) are enhanced under tensile strain due to the larger hybridization with Cr d states near the E_F with tensile strain. As can be seen from Fig. 5(d),

the term of $|\langle p_y^-|L_z|p_x^+\rangle|^2$ displays more remarkable change with strain than $|\langle p_y^-|L_x|p_z^+\rangle|^2$, which results in an enhanced in-plane MCA in ML 1T-$CrTe_2$ under the tensile strains.

The effect of on-site U on the modulation of MCA is also investigated at the lattice constant of a_{DFT}. As shown in Fig. S11(b) of SM [35], the magnetic easy axis switches from in-plane (−1.40 meV/Cr) to out-of-plane (4.77 meV/Cr) direction with increasing U from 0 to 5 eV. We also note that for Cr d orbitals, the main occupied state $e_g'^+$ shifts down, while the main unoccupied state $e_g'^-$ moves up (see Fig. S13(a) of SM [35]), which significantly suppresses the negative contribution from $|\langle e_g'^+|L_z|e_g'^-\rangle|^2$. The electronic features of Te p orbitals are also affected by U due to the hybridization with Cr d states despite no on-site U on them. The positive contribution from $|\langle p_y^-|L_x|p_z^+\rangle|^2$ is enhanced due to the larger weight of p_y^- near E_F and decreased energy difference between p_y^- and p_z^+. The orbital interaction profile between p_y and p_x is notably different for $U = 0$ eV and $U = 5$ eV cases. The otherwise negative contribution from $|\langle p_y^-|L_z|p_x^+\rangle|^2$ changes to spin-conserving transition $|\langle p_y^-|L_z|p_x^-\rangle|^2$ owing to the variation of Te p_x with U, which positively contributes to the MCA when $U = 5$ eV [see Fig. 5(e) and Fig. S13(b)]. The overall out-of-plane MCA is therefore enhanced with increasing U.

IV. CONCLUSION

In summary, the magnetic properties of ML 1T-$CrTe_2$ have been systematically studied from first principles, which is controversial in previous studies. The magnetic ground of ML 1T-$CrTe_2$ is tunable among FM, sAFM-*AABB*, and AFM-*Z* configurations in the range of the applied strain ($-4 \sim 4\%$) and U values ($0 \sim 5$ eV). We reveal that the modulation of the magnetism originates from the different responses of the AFM Cr-Cr direct exchange interactions and the FM Cr-Te-Cr superexchange interactions to strain and U. The strain and U effect on the magnetic exchange interactions have been thoroughly examined by means of spin-lattice coupling, TB analysis, structural changes, and GKA model. We show that the BQ exchange interactions are important to fundamentally understand the magnetism of ML 1T-$CrTe_2$, which plays a key role in stabilizing the FM and sAFM-*AABB* states. Our study elucidates the diverse magnetic ground states observed in $CrTe_2$ and their dependences on strain and electronic correlation, which may be beneficial for the tuning of 2D materials for spintronic devices through strain or Coulomb engineering. These insights may guide future research to design and manipulate the electronic and magnetic properties in similar materials, and contribute the development of spintronics devices based on these materials.

ACKNOWLEDGMENTS

This work was supported by the Ministry of Science and Technology of the People´s Republic of China (Grant No. 2022YFA1402903), the National Natural Science Foundation of China under Grants Nos. 12004160 and 12104518. Z.G. also acknowledges the financial support from Shenzhen Science and Technology Program (Grant No. KQTD20190929173815000), Guangdong Innovative and Entrepreneurial Research Team Program (Grant No. 2019ZT08C044), and the Guangdong Provincial Key Laboratory of Computational Science and Material Design(Grant No. 2019B030301001). Part of this work was supported by the Quantum Science Center of Guangdong-Hong Kong-Macao Greater Bay Area (Guangdong) and the Open Project of Guangdong Provincial Key Laboratory of Magnetoelectric Physics and Devices, Grant No. 2022B1212010008. Computational time was supported by the Center for Computational Science and Engineering of Southern University of Science and Technology and the Major Science and Technology Infrastructure Project of Material Genome Big-science Facilities Platform supported by Municipal Development and Reform Commission of Shenzhen.

[1] C. Gong, L. Li, Z. Li, H. Ji, A. Stern, Y. Xia, T. Cao, W. Bao, C. Wang, Y. Wang *et al.*, Discovery of intrinsic ferromagnetism in two-dimensional van der Waals crystals, Nature (London) **546**, 265 (2017).

[2] B. Huang, G. Clark, E. Navarro-Moratalla, D. R. Klein, R. Cheng, K. L. Seyler, D. Zhong, E. Schmidgall, M. A. McGuire, D. H. Cobden *et al.*, Layer-dependent ferromagnetism in a van der Waals crystal down to the monolayer limit, Nature (London) **546**, 270 (2017).

[3] M.-W. Lin, H. L. Zhuang, J. Yan, T. Z. Ward, A. A. Puretzky, C. M. Rouleau, Z. Gai, L. Liang, V. Meunier, B. G. Sumpter *et al.*, Ultrathin nanosheets of $CrSiTe_3$: A semiconducting two-dimensional ferromagnetic material, J. Mater. Chem. C **4**, 315 (2016).

[4] Y. Deng, Y. Yu, Y. Song, J. Zhang, N. Z. Wang, Z. Sun, Y. Yi, Y. Z. Wu, S. Wu, J. Zhu *et al.*, Gate-tunable room-temperature ferromagnetism in two-dimensional Fe_3GeTe_2, Nature (London) **563**, 94 (2018).

[5] A. F. May, S. Calder, C. Cantoni, H. Cao, and M. A. McGuire, Magnetic structure and phase stability of the van der Waals bonded ferromagnet $Fe_{3-x}GeTe_2$, Phys. Rev. B **93**, 014411 (2016).

[6] W. Liu, L. He, Y. Xu, K. Murata, M. C. Onbasli, M. Lang, N. J. Maltby, S. Li, X. Wang, C. A. Ross *et al.*, Enhancing magnetic ordering in Cr-doped Bi_2Se_3 using high-T_C ferrimagnetic insulator, Nano Lett. **15**, 764 (2015).

[7] S. Liu, X. Yuan, Y. Zou, Y. Sheng, C. Huang, E. Zhang, J. Ling, Y. Liu, W. Wang, C. Zhang *et al.*, Wafer-scale two-dimensional ferromagnetic Fe_3GeTe_2 thin films grown by molecular beam epitaxy, npj 2D Mater. Appl. **1**, 30 (2017).

[8] Q. Li, M. Yang, C. Gong, R. V. Chopdekar, A. T. N'Diaye, J. Turner, G. Chen, A. Scholl, P. Shafer, E. Arenholz *et al.*, Patterning-induced ferromagnetism of Fe_3GeTe_2 van der Waals materials beyond room temperature, Nano Lett. **18**, 5974 (2018).

[9] M. Bonilla, S. Kolekar, Y. Ma, H. C. Diaz, V. Kalappattil, R. Das, T. Eggers, H. R. Gutierrez, M.-H. Phan, and M. Batzill, Strong room-temperature ferromagnetism in VSe_2 monolayers on van der Waals substrates, Nat. Nanotechnol. **13**, 289 (2018).

[10] D. J. O'Hara, T. Zhu, A. H. Trout, A. S. Ahmed, Y. K. Luo, C. H. Lee, M. R. Brenner, S. Rajan, J. A. Gupta, D. W. McComb, and R. K. Kawakami, Room temperature intrinsic ferromagnetism in epitaxial manganese selenide films in the monolayer limit, Nano Lett. **18**, 3125 (2018).

[11] D. C. Freitas, R. Weht, A. Sulpice, G. Remenyi, P. Strobel, F. Gay, J. Marcus, and M. Nunez-Regueiro, Ferromagnetism in layered metastable $1T$-$CrTe_2$, J. Phys.: Condens. Matter **27**, 176002 (2015).

[12] X. Sun, W. Li, X. Wang, Q. Sui, T. Zhang, Z. Wang, L. Liu, D. Li, S. Feng, S. Zhong *et al.*, Room temperature ferromagnetism in ultra-thin van der Waals crystals of $1T$-$CrTe_2$, Nano Res. **13**, 3358 (2020).

[13] X. Zhang, Q. Lu, W. Liu, W. Niu, J. Sun, J. Cook, M. Vaninger, P. F. Miceli, D. J. Singh, S. W. Lian *et al.*, Room-temperature intrinsic ferromagnetism in epitaxial $CrTe_2$ ultrathin films, Nat. Commun. **12**, 2492 (2021).

[14] F. Fabre, A. Finco, A. Purbawati, A. Hadj-Azzem, N. Rougemaille, J. Coraux, I. Philip, and V. Jacques, Characterization of room-temperature in-plane magnetization in thin flakes of $CrTe_2$ with a single-spin magnetometer, Phys. Rev. Mater. **5**, 034008 (2021).

[15] Y. Sun, P. Yan, J. Ning, X. Zhang, Y. Zhao, Q. Gao, M. Kanagaraj, K. Zhang, J. Li, X. Lu *et al.*, Ferromagnetism in two-dimensional $CrTe_2$ epitaxial films down to a few atomic layers, AIP Adv. **11**, 2492 (2021).

[16] J.-J. Xian, C. Wang, R. Li, M. Han, J. Lin, W.-H. Zhang, Z.-Y. Liu, Z.-M. Zhang, J.-H. Nie, W. Ji *et al.*, Spin mapping of intralayer antiferromagnetism and spin-flop transition in monolayer $CrTe_2$, Nat. Commun. **13**, 257 (2022).

[17] X. Yang, X. Zhou, W. Feng, and Y. Yao, Tunable magneto-optical effect, anomalous Hall effect, and anomalous Nernst effect in the two-dimensional room-temperature ferromagnet $1T$-$CrTe_2$, Phys. Rev. B **103**, 024436 (2021).

[18] S. Li, S.-S. Wang, B. Tai, W. Wu, B. Xiang, X.-L. Sheng, and S. A. Yang, Tunable anomalous Hall transport in bulk and two-dimensional $1T$-$CrTe_2$: A first-principles study, Phys. Rev. B **103**, 045114 (2021).

[19] L. Wu, L. Zhou, X. Zhou, C. Wang, and W. Ji, In-plane epitaxy-strain-tuning intralayer and interlayer magnetic coupling in $CrSe_2$ and $CrTe_2$ monolayers and bilayers, Phys. Rev. B **106**, L081401 (2022).

[20] A. Otero Fumega, J. Phillips, and V. Pardo, Controlled two-dimensional ferromagnetism in $1T$-$CrTe_2$: The role of charge density wave and strain, J. Phys. Chem. C **124**, 21047 (2020).

[21] N. Abuawwad, M. dos Santos Dias, H. Abusara, and S. Lounis, Noncollinear magnetism in two-dimensional $CrTe_2$, J. Phys.: Condens. Matter **34**, 454001 (2022).

[22] L. Meng, Z. Zhou, M. Xu, S. Yang, K. Si, L. Liu, X. Wang, H. Jiang, B. Li, P. Qin *et al.*, Anomalous thickness dependence of Curie temperature in air-stable two-dimensional ferromagnetic $1T$-$CrTe_2$ grown by chemical vapor deposition, Nat. Commun. **12**, 809 (2021).

[23] H. Y. Lv, W. J. Lu, D. F. Shao, Y. Liu, and Y. P. Sun, Strain-controlled switch between ferromagnetism and antiferromagnetism in 1T-CrX_2 (X = Se,Te) monolayers, Phys. Rev. B **92**, 214419 (2015).

[24] M. Huang, Z. Ma, S. Wang, S. Li, M. Li, J. Xiang, P. Liu, G. Hu, Z. Zhang, Z. Sun *et al.*, Significant perpendicular magnetic anisotropy in room-temperature layered ferromagnet of Cr-intercalated $CrTe_2$, 2D Mater. **8**, 031003 (2021).

[25] M. A. McGuire, Crystal and magnetic structures in layered, transition metal dihalides and trihalides, Crystals **7**, 121 (2017).

[26] A. Kartsev, M. Augustin, R. F. L. Evans, K. S. Novoselov, and E. J. G. Santos, Biquadratic exchange interactions in two-dimensional magnets, npj Comput. Mater **6**, 150 (2020).

[27] J. Y. Ni, X. Y. Li, D. Amoroso, X. He, J. S. Feng, E. J. Kan, S. Picozzi, and H. J. Xiang, Giant biquadratic exchange in 2D magnets and its role in stabilizing ferromagnetism of $NiCl_2$ monolayers, Phys. Rev. Lett **127**, 247204 (2021).

[28] G. Kresse and J. Furthmüller, Efficient iterative schemes for ab initio total-energy calculations using a plane-wave basis set, Phys. Rev. B **54**, 11169 (1996).

[29] J. P. Perdew, K. Burke, and M. Ernzerhof, Generalized gradient approximation made simple, Phys. Rev. Lett **77**, 3865 (1996).

[30] P. E. Blöchl, Projector augmented-wave method, Phys. Rev. B **50**, 17953 (1994).

[31] I. A. Vladimir, F. Aryasetiawan, and A. I. Lichtenstein, First-principles calculations of the electronic structure and spectra of strongly correlated systems: The LDA+U method, J. Phys.: Condens. Matter **9**, 767 (1997).

[32] S. L. Dudarev, G. A. Botton, S. Y. Savrasov, C. J. Humphreys, and A. P. Sutton, Electron-energy-loss spectra and the structural stability of nickel oxide: An LSDA+U study, Phys. Rev. B **57**, 1505 (1998).

[33] D. J. Chadi, Special points for Brillouin-zone integrations, Phys. Rev. B **16**, 1746 (1977).

[34] G. Pizzi, V. Vitale, R. Arita, S. Bluegel, F. Freimuth, G. Geranton, M. Gibertini, D. Gresch, C. Johnson, T. Koretsune *et al.*, Wannier90 as a community code: New features and applications, J. Phys.: Condens. Matter **32**, 165902 (2020).

[35] See Supplemental Material at http://link.aps.org/supplemental/10.1103/PhysRevB.108.144404 for details on the magnetic properties of ML $1T$-$CrTe_2$ and Refs. [39,45].

[36] S. Landron and M.-B. Lepetit, Importance of t_{2g}-e_g hybridization in transition metal oxides, Phys. Rev. B **77**, 125106 (2008).

[37] P. Gao, X. Li, and J. Yang, Thickness dependent magnetic transition in few layer 1T phase $CrTe_2$, J. Phys. Chem. Lett. **12**, 6847 (2021).

[38] D. Amoroso, P. Barone, and S. Picozzi, Spontaneous skyrmionic lattice from anisotropic symmetric exchange in a Ni-halide monolayer, Nat. Commun. **11**, 5784 (2020).

[39] J. Li, J. Feng, P. Wang, E. Kan, and H. Xiang, Nature of spin-lattice coupling in two-dimensional CrI_3 and $CrGeTe_3$, Sci. China: Phys., Mech. Astron. **64**, 286811 (2021).

[40] P. W. Anderson, Antiferromagnetism. Theory of superexchange interaction, Phys. Rev. **79**, 350 (1950).

[41] J. Kanamori, Superexchange interaction and symmetry properties of electron orbitals, J. Phys. Chem. Solids **10**, 87 (1959).

[42] A. K. Jena, S. K. Mallik, M. C. Sahu, S. Sahoo, A. K. Sahoo, N. K. Sharma, J. Mohanty, S. K. Gupta, R. Ahuja, and S. Sahoo,

Strain-mediated ferromagnetism and low-field magnetic reversal in Co doped monolayer WS_2, Sci. Rep. **12**, 2593 (2022).

[43] H. Zhu, Y. Gao, Y. Hou, Z. Gui, and L. Huang, Tunable magnetic anisotropy in two-dimensional CrX_3/AlN (X = I, Br, Cl) heterostructures, Phys. Rev. B **106**, 134412 (2022).

[44] L. M. Sandratskii, Noncollinear magnetism in itinerant-electron systems: Theory and applications, Adv. Phys. **47**, 91 (1998).

[45] S. Toth and B. Lake, Linear spin wave theory for single-Q incommensurate magnetic structures, J. Phys.: Condens. Matter **27**, 166002 (2015).

[46] J. Zhou, X. Song, J. Chai, N. L. M. Wong, X. Xu, Y. Jiang, Y. P. Feng, M. Yang, and S. Wang, Structure dependent and strain tunable magnetic ordering in ultrathin chromium telluride, J. Alloys Compd. **893**, 162223 (2022).